This is the accepted manuscript made available via CHORUS. The article has been published as:

Chirality, band structure, and localization in waveguide quantum electrodynamics

Imran M. Mirza, Jeremy G. Hoskins, and John C. Schotland

Phys. Rev. A **96**, 053804 — Published 2 November 2017

DOI: 10.1103/PhysRevA.96.053804

Chirality, Band Structure and Localization in Waveguide Quantum Electrodynamics

Imran M. Mirza

Department of Physics, University of Michigan, Ann Arbor, Michigan 48109, USA

Jeremy G. Hoskins

Department of Mathematics, University of Michigan, Ann Arbor, Michigan 48109, USA

John C. Schotland

Department of Mathematics and Department of Physics,

University of Michigan, Ann Arbor, Michigan 48109, USA

Abstract

Architectures based on waveguide quantum electrodynamics have emerged as promising candidates for quantum networks. In this paper, we analyze the propagation of single-photons in disordered many-atom waveguides. We pay special attention to the influence of chirality (directionality of photon transport) on the formation of localized photonic states, considering separately the cases of disorder in the atomic positions and in the atomic transition frequencies.

I. INTRODUCTION

The investigation of light-matter interactions in quantum optics is largely concerned with the study of systems consisting of a small number of atoms [1]. However, experiments with cold atom systems [2, 3] have led to the study of light propagation in media consisting of a large number of densely-packed scatterers [4–6]. Moroever, given the remarkable progress on the scalability of nanophotonic systems in cavity quantum electrodynamics (QED) [7] and ion-trapping techniques [8], the control of quantum states of light coupled to complex atomic media with tunable properties seems to be not far away.

Multi-atom waveguide QED provides a convenient platform to investigate light propagation in complex atomic media. In addition, enhancement of spin-orbit coupling of light in nanoscale waveguides leads to the remarkable ability to control the direction of light propagation [9]. In so-called chiral waveguides, light can propagate preferentially in one direction. Due to this feature, entanglement generation and control [10, 11], photon-photon correlations [12], superradiance/subradiance [13], and selective radiance [14] have been extensively investigated.

Relatively little attention has been paid to the topic of single-photon transport in many-body waveguide QED systems. Shen et al. developed a transfer matrix approach for periodic systems of two-level atoms [15]. Witthaut et al. extended this work to the case of three-level atoms and considered the effects of position disorder on single photon transport [16]. More recently, Marcuzzi et al. [17] investigated position-disordered Rydberg atom systems in tight optical traps. Their experiments were performed for a linear array of up to eight optical tweezers, each containing a single atom, and provided evidence for disorder-induced suppression of excitation transfer.

In the setting of periodic multi-atom waveguide QED, an important question is to characterize the formation of allowed and forbidden bands for single photon transport. This topic has been addressed for symmetric waveguides [18–20]. However, the extent to which chirality can influence band structure and dispersion has not been addressed. In this work, we show that a small chiral imbalance in group velocities can change the location and width of bands compared to symmetric waveguide systems.

Anderson localization was first discussed in the context of disordered electronic systems [21]. Later, the phenomenon has also been extensively investigated in a variety of

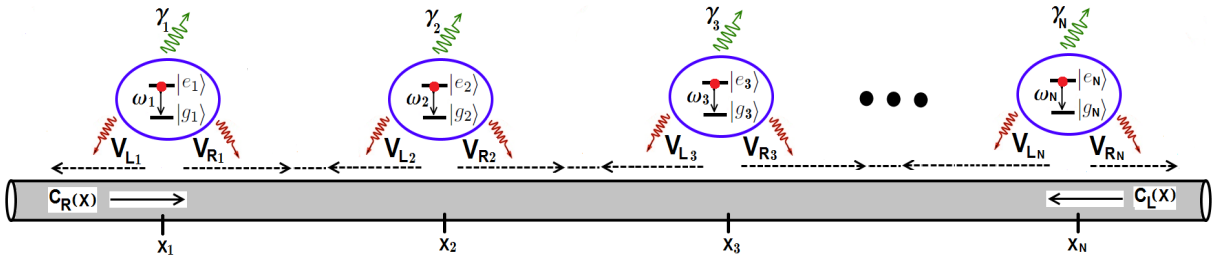

FIG. 1: (Color online) Illustrating the waveguide QED system that is considered in this paper.

fields including acoustics, elasticity and optics. In classical optics, in addition to Refs.[22–24], Anderson himself analyzed the problem of localization of electromagnetic waves [25]. More recently, localization has received considerable attention in quantum optical and nanophotonic systems. For instance, Sapienza et al. have experimentally demonstrated that atom-photon coupling can be enhanced in cavity QED systems by adding lithographically controlled disorder in photonic crystal waveguides [26]. Moreover, waveguide QED provides a platform to study photon localization due to the competition between long-ranged waveguide mediated atomic interactions and atomic disorder with short-ranged correlations. Note that such competition is generally not present in other quantum optical architectures [27–29].

In this paper, we consider chiral and bidirectional waveguides containing 10–10^3 two-level atoms. The effects of two types of disorder are examined: randomness in atomic positions and in atomic transition frequencies. In both cases, we study the single-photon transmission coefficient and localization length as a function of the atom-field detuning and the strength of the disorder. For chiral waveguides, we find that photon transport is immune to position disorder. However, for frequency disorder localization does occur. For bidirectional waveguides, both types of disorder lead to localization.

The paper is organized as follows. In section II we consider the theory of chiral waveguides and discuss photon transport in both periodic and disordered settings. In Section III, we focus on the non-chiral situation. In Section IV and V, we discuss the band structure and disorder respectively, for both small and symmetric waveguide problems. Finally, in Section VI, we close with a discussion of our results.

II. CHIRAL WAVEGUIDES

When confined to subwavelength scales, light shows the remarkable feature of enhanced spin-orbit coupling, enabling the creation of chiral waveguides. Here, chirality is defined as an imbalance in the left and right waveguide emission directions or atom-field coupling strength [9, 30–32]. In recent years, chiral waveguide QED has undergone tremendous development [30, 33] in which up to 90% directionality has been reported. We note that chiral waveguides are similar to a waveguide-coupled ring resonators, in which light propagation is also unidirectional [34].

In this paper we consider the following scenario for both chiral and bidirectional waveguides. A collection of two-level atoms (also referred to as qubits or emitters) is side-coupled to a one-dimensional lossless and dispersionless waveguide. This model can be experimentally realized in a number of different physical settings including cadmium selenide quantum dots interacting with silver nanowires [35], Josephson junctions in microwave transmission lines [36], Cesium atoms coupled to photonic crystal waveguide [13], and silicon-vacancy color centers coupled to diamond nanowaveguides [37].

We consider the following Hamiltonian for a multiatom chiral waveguide system as illustrated in Fig.1 with $V_{L_j} = 0$ and $V_{R_j} = V_j$:

$$\begin{aligned}\hat{H} = &\sum_j (\omega_j - i\gamma_j)\hat{\sigma}_j^\dagger \hat{\sigma}_j + \int dx \hat{c}^\dagger(x) \left(\omega_0 - iv_g \frac{\partial}{\partial x}\right) \hat{c}(x) \\ &+ \sum_j \int dx \delta(x - x_j) \left[V_j \hat{c}^\dagger(x)\hat{\sigma}_j + h.c.\right] \ .\end{aligned} \tag{1}$$

The first term in (1) corresponds to the Hamiltonian of the atoms, the second term to the Hamiltonian of the quantized field, and the third term to the interaction between the atoms and the field. Here we work in units where $\hbar = 1$, have employed the method of real-space quantization [15, 38] and have made the rotating wave approximation. The position of the jth atom is denoted x_j and its transition frequency is ω_j with $j = 1, \ldots, N$. In addition, ω_0 is the frequency around which waveguide dispersion relation has been linearized, v_g is the group velocity of the photon in the waveguide and γ_j is the rate of spontaneous emission of the jth atom. The atomic lowering operator is denoted $\hat{\sigma}_j$ and the field operator $\hat{c}(x)$ annihilates a photon at the position x. The nonvanishing commutation relations are given

by

$$\left[\hat{c}(x), \hat{c}^\dagger(x')\right] = \delta(x - x') \ , \quad \{\hat{\sigma}_i, \hat{\sigma}_j^\dagger\} = \delta_{ij} \ . \tag{2}$$

Finally, V_j is the evanescent coupling of the atom to the waveguide continuum.

The quantum state of the system in the subspace of zero and one excitations is of the form

$$|\Psi\rangle = \int dx \varphi(x) \hat{c}^\dagger(x) \, |\varnothing\rangle + \sum_j a_j \hat{\sigma}_j^\dagger \, |\varnothing\rangle \ , \tag{3}$$

where a_j is the probability amplitude for the jth atom, $\varphi(x)$ is the one-photon amplitude and $|\varnothing\rangle$ is the ground state of the atom-waveguide system. The equations obeyed by a and φ can be obtained by substituting the above expression for $|\Psi\rangle$ into the time-independent Schrödinger equation $\hat{H} \, |\Psi\rangle = \hbar\omega \, |\Psi\rangle$, where ω is the frequency of the photon. We thus obtain

$$-iv_g \frac{\partial \varphi(x)}{\partial x} + \sum_{j=1}^{N} V_j a_j \delta(x - x_j) = (\omega - \omega_0) \, \varphi(x) \ , \tag{4a}$$

$$V_j^* \varphi(x_j) = (\omega - \omega_j + i\gamma_j) a_j \ . \tag{4b}$$

Eliminating a_j from (4a) yields the following equation for φ:

$$-iv_g \frac{\partial \varphi(x)}{\partial x} + \sum_{j=1}^{N} v_j \delta(x - x_j) \varphi(x) = (\omega - \omega_0) \varphi(x), \tag{5}$$

where $v_j = |V_j|^2 / (\omega - \omega_j - i\gamma_j)$. The solution to (5) can be obtained by observing that in between the atoms, when $x \neq x_j$, $\varphi(x) = Ae^{iqx}$, where the wavenumber $q = (\omega - \omega_0)/v_g$ and A is constant. Thus φ is of the form

$$\varphi(x) = \begin{cases} e^{iqx}, & x < x_1, \\ t_1 e^{iqx}, & x_1 \leq x \leq x_2, \\ \vdots & \\ t_N e^{iqx}, & x > x_N. \end{cases} \tag{6}$$

To obtain the coefficients t_j, we integrate (5) over the interval $[x_j - \epsilon, x_j + \epsilon]$, where ϵ is a small positive number. This yields the jump condition

$$iv_g[\varphi(x_j + \epsilon) - \varphi(x_j - \epsilon)] = v_j \varphi(x_j). \tag{7}$$

Next, we regularize the discontinuity in φ according to

$$\varphi(x_j) = \lim_{\epsilon \longrightarrow 0} \left[\varphi(x_j + \epsilon) + \varphi(x_j - \epsilon)\right]/2 \tag{8}$$

and introduce the quantity $\Gamma_j = |V_j|^2/2v_g$. Eq. (7) thus becomes

$$\varphi(x_j + \epsilon) = T_j \varphi(x_j - \epsilon), \tag{9}$$

where

$$T_j = \frac{\omega - \omega_j + i(\gamma_j - \Gamma_j)}{\omega - \omega_j + i(\gamma_j + \Gamma_j)}. \tag{10}$$

Finally, by using (6) we arrive at the recursion relation

$$t_j = T_j t_{j-1}, \tag{11}$$

which allows us to determine the amplitude φ.

To study the transport of single photons, we define the transmission coefficient $T = |\varphi(x_N)/\varphi(x_1)|^2$, which upon making use of (6) and (11) becomes

$$T = \prod_{j=1}^{N} |T_j|^2 \ . \tag{12}$$

As expected, if $\gamma_j = 0$ (no losses), then $T = 1$ and the system behaves as an all-pass filter.

A. Periodic arrangement

Eq. (11) is applicable to both periodic and disordered arrangements of atoms. In the periodic case, unlike the bidirectional setting discussed in section III, there is no band structure and the transmission is independent of the period. On the other hand, it is convenient to distinguish three regimes when $\gamma_j \neq 0$: undercoupled ($\gamma_j > \Gamma_j$), overcoupled ($\gamma_j < \Gamma_j$), and critically coupled ($\gamma_j = \Gamma_j$). As is evident from the single atom case, which we show in Fig. 2(a), in the critical coupling regime the transmission reaches its minimum value. In Fig. 2(b), we plot the transmission for different numbers of identical atoms in the critical coupling regime. As we increase the number of atoms, we notice the width of the region of low transmission grows and for a 100-atom chain, transmission is suppressed for a wide range of frequencies.

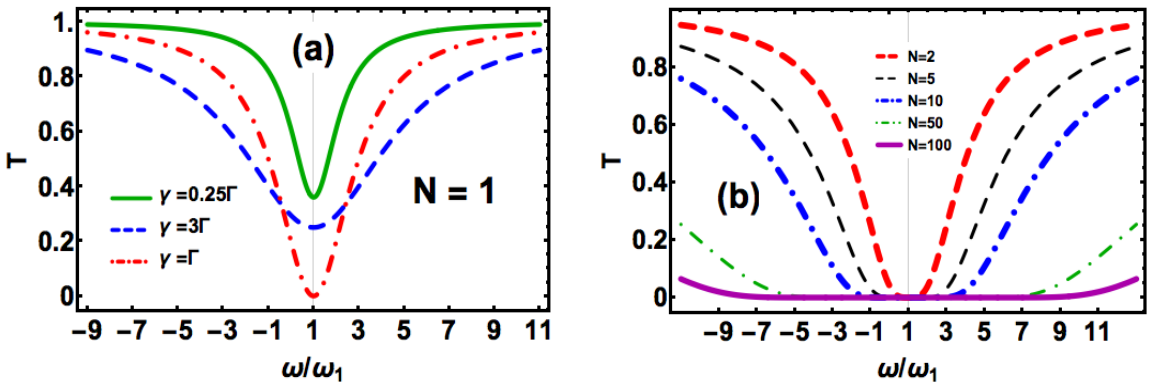

FIG. 2: (Color online) Transmission of a single photon in a chiral system consisting of (a) 1 and (b) 2, 5, 10, 50 and 100 periodically arranged identical atoms ($\omega_j = \omega_1$ and $\gamma_j = \gamma$ for all j). In (a) the solid green, red dotted-dashed and blue dashed lines represent the over-, critical- and under-coupled regimes, respectively. In (b) we have chosen the critical coupling case with $\gamma = \Gamma$.

B. Disordered arrangement

We now introduce disorder in the multi-atom chain and investigate the occurence of single photon localization. For recent studies on localization in photonic systems, see for instance [27–29, 39, 40]. In what follows and for the rest of the paper, all random variables are generated from a Gaussian probability density of the form

$$P(x) = \frac{1}{\sqrt{2\pi\sigma^2}} e^{-(x-\overline{x})^2/2\sigma^2}, \tag{13}$$

where $\overline{x}$ is the mean and σ being the standard deviation is a measure of the strength of the disorder.

1. *Frequency disorder*

Here we consider the case of frequency disorder, in which we assume that the atomic transition frequencies are random. This type of disorder can be present in optically trapped Rydberg atoms, either due to non-uniformity of the applied potential or when beam focusing is inhomogeneous [41, 42]. We begin by calculating the average transmission and then compute the localization length.

Suppose that the detunings $\delta_j = \omega - \omega_j$ are independent and identically distributed Gaussian random variables. Making use of (10) and (11), we find that the average transmission for an N-atom chain is given by

$$\langle T \rangle = \int \prod_{j=1}^{N} d\delta_j P(\delta_j) |T_j|^2 \tag{14}$$

$$= \langle |\tau|^2 \rangle^N. \tag{15}$$

Here

$$\langle |\tau|^2 \rangle = \int d\delta P(\delta) |\tau|^2, \tag{16}$$

where

$$\tau = \frac{\delta + i(\gamma - \Gamma)}{\delta + i(\gamma + \Gamma)}. \tag{17}$$

It is easily seen that

$$|\tau|^2 = 1 - \left[(\gamma + \Gamma)^2 - (\gamma - \Gamma)^2 \right] \int_0^\infty e^{-\lambda\left(\delta^2 + (\gamma+\Gamma)^2\right)} d\lambda. \tag{18}$$

Carrying out the indicated average over δ with $\langle \delta \rangle = \bar{\delta}$ yields

$$\langle |\tau|^2 \rangle = 1 - 4\gamma\Gamma \int_0^\infty \frac{\exp\left[-\lambda(\gamma + \Gamma)^2 - \frac{\lambda \bar{\delta}^2}{1 + 2\lambda\sigma^2} \right]}{\sqrt{1 + 2\lambda\sigma^2}} d\lambda, \tag{19}$$

which allows us to calculate the average transmission from (15) .

By analogy to the theory of disordered electronic systems [43–45], we define the localization length ξ by

$$\xi^{-1} = -\lim_{N \to \infty} \frac{\langle \ln T \rangle}{N} \ , \tag{20}$$

where the average is over all detunings δ_j. It is easily seen from (12) and (18) that

$$\langle \ln T \rangle = N \langle \ln |\tau|^2 \rangle \tag{21}$$

and thus

$$\xi^{-1} = -\langle \ln |\tau|^2 \rangle. \tag{22}$$

In the critical coupling regime with $\gamma = \Gamma$, we can perform the above average explicitly and thus obtain

$$\xi^{-1} = -\frac{2\Gamma}{\sqrt{2\pi\sigma^2}} \int_{-\infty}^{\infty} \ln\left(1 - \frac{1}{1 + x^2} \right) e^{-(2\Gamma x - \bar{\delta})^2 / 2\sigma^2} dx. \tag{23}$$

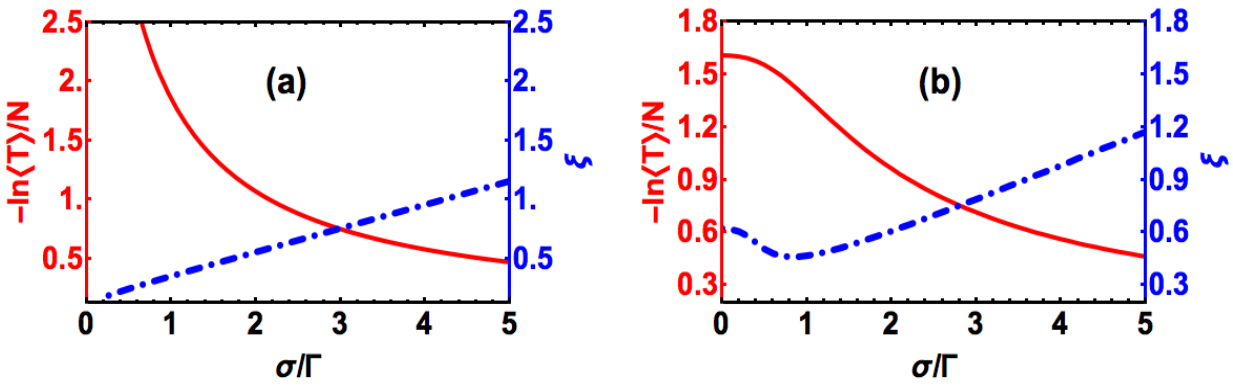

FIG. 3: (Color online) Average transmission and localization length for a frequency-disordered chiral waveguide in the critical coupling regime. (a) $\bar{\delta} = 0$ and (b) $\bar{\delta} = \Gamma$.

In Fig. 3, we plot the average transmission and localization length as a function of the strength of the disorder σ and the average detuning $\bar{\delta}$. We first consider the case $\bar{\delta} = 0$. We find that the system is purely reflecting ($\langle T \rangle = 0$) when $\sigma = 0$. This is a consequence of the fact that the system is both on resonance and critically coupled. We note that as σ is increased the transmission increases, as does the localization length. Next we consider the case $\bar{\delta} = \Gamma$. Here we see that even when $\sigma = 0$, the system is off resonance and the average transmission is nonvanishing. Note the presence of a minimum in the localization length near $\sigma = \Gamma$.

2. Position disorder

We now consider the effect of position disorder of the atoms in the chain. It follows immediately from (12) that the transmission T does not depend on the position of the atoms. Thus in chiral waveguides we see that transport is immune to position disorder.

III. BI-DIRECTIONAL WAVEGUIDES

We consider the following Hamiltonian for a multiatom bidirectional waveguide

$$\hat{H} = \sum_j (\omega_j - i\gamma_j)\hat{\sigma}_j^\dagger \hat{\sigma}_j + \int dx \hat{c}_R^\dagger(x) \left(\omega_0 - iv_R \frac{\partial}{\partial x}\right) \hat{c}_R(x) + \int dx \hat{c}_L^\dagger(x) \left(\omega_0 + iv_L \frac{\partial}{\partial x}\right) \hat{c}_L(x) + \sum_{m,j} \int dx \delta(x - x_j) \left[V_{mj} \hat{c}_m^\dagger(x) \hat{\sigma}_j + h.c.\right]. \tag{24}$$

The first term in (24) is the Hamiltonian of the atoms. The second and third terms are the Hamiltonian of the waveguide, which supports left- and right-going modes with group velocities v_R and v_L, respectively. Here the the sum is over $m \in \{R, L\}$. The destruction of a single photon in the left (right) waveguide continuum at position x is represented by the field operator $\hat{c}_L(x)(\hat{c}_R(x))$. The nonvanishing commutation relations for field operators are given by

$$\left[\hat{c}_m(x), \hat{c}_n^\dagger(x')\right] = \delta_{mn}\delta(x - x'). \tag{25}$$

The third term in (24) accounts for the interaction between the quantized field and the atoms, with V_{mj} denoting the corresponding coupling, which is chosen to be real-valued. The waveguide described by the Hamiltonian (24) is said to be *bidirectional*. If $v_R = v_L$ and $V_{Rj} = V_{Lj}$ the waveguide is referred to as *symmetric*. Evidently, the extreme case with either v_R or v_L vanishing corresponds to a chiral waveguide.

We consider a one-photon quantum state of the form

$$|\Psi\rangle = \sum_m \int dx \varphi_m(x) \hat{c}_m^\dagger(x) |\varnothing\rangle + \sum_j a_j \hat{\sigma}_j^\dagger |\varnothing\rangle. \tag{26}$$

Here $\varphi_R(x), (\varphi_L(x))$ is the one-photon amplitude in the right (left) waveguide continuum. As in section II, the equations obeyed by the amplitudes can be obtained from the Schrödinger equation. We thus obtain

$$-iv_R \frac{\partial \varphi_R(x)}{\partial x} + \sum_{j=1}^N V_{R_j} a_j \delta(x - x_j) = (\omega - \omega_0)\varphi_R(x), \tag{27a}$$

$$iv_L \frac{\partial \varphi_L(x)}{\partial x} + \sum_{j=1}^N V_{L_j} a_j \delta(x - x_j) = (\omega - \omega_0)\varphi_L(x), \tag{27b}$$

$$V_{R_j}\varphi_R(x_j) + V_{L_j}\varphi_L(x_j) = (\omega - \omega_j + i\gamma_j)a_j. \tag{27c}$$

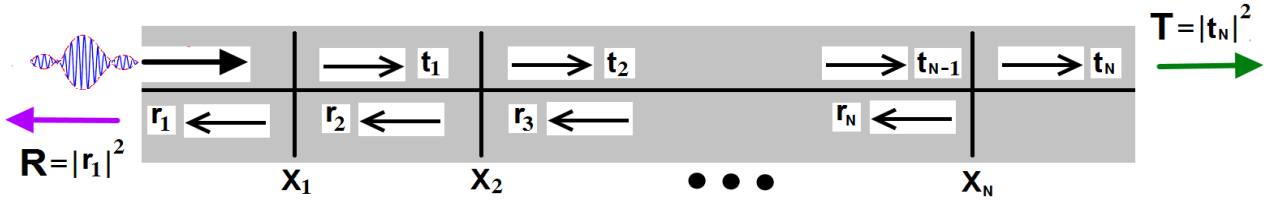

FIG. 4: (Color online) Illustrating the transmission and reflection amplitudes at the location of each atom.

Eliminating a_j from the above, we find that the following equations are obeyed by φ_R and φ_L:

$$-iv_R\frac{\partial\varphi_R(x)}{\partial x}+\sum_j\frac{V_{R_j}\delta(x-x_j)}{\omega-\omega_j+i\gamma_j}\Big(V_{R_j}\varphi_R(x)+V_{L_j}\varphi_L(x)\Big)=(\omega-\omega_0)\varphi_R(x), \tag{28a}$$

$$iv_L\frac{\partial\varphi_L(x)}{\partial x}+\sum_j\frac{V_{L_j}\delta(x-x_j)}{\omega-\omega_j+i\gamma_j}\Big(V_{R_j}\varphi_R(x)+V_{L_j}\varphi_L(x)\Big)=(\omega-\omega_0)\varphi_L(x), \tag{28b}$$

When $x\neq x_j$, the amplitudes $\varphi_R(x)$ and $\varphi_L(x)$ are given by $\varphi_R(x)=A_Re^{iq_Rx}$ and $\varphi_L(x)=A_Le^{-iq_Lx}$. Here $q_R=(\omega-\omega_0)/v_R$, $q_L=(\omega-\omega_0)/v_L$ are the wavenumbers associated with the right and left field amplitudes, respectively, and A_R and A_L are constant. Thus, we obtain

$$\varphi_R(x)=\begin{cases}e^{iq_Rx}, & x<x_1,\\ t_1e^{iq_Rx}, & x_1\le x\le x_2,\\ \vdots & \\ t_Ne^{iq_Rx}, & x>x_N.\end{cases} \tag{29}$$

and

$$\varphi_L(x)=\begin{cases}r_1e^{-iq_Lx}, & x<x_1,\\ r_2e^{-iq_Lx}, & x_1\le x\le x_2,\\ \vdots & \\ r_Ne^{-iq_Lx}, & x_{N-1}\le x\le x_N,\\ 0, & x>x_N.\end{cases} \tag{30}$$

where $r_{N+1}=0$ and $t_0=1$. See Fig. 4. In order to obtain the coefficients t_j and r_j we

integrate (28) over the interval $[x_j-\epsilon, x_j+\epsilon]$, which yields the jump conditions

$$-iv_R\Big[\varphi_R(x_j+\epsilon)-\varphi_R(x_j-\epsilon)\Big]+\frac{V_{R_j}}{\omega-\omega_j+i\gamma_j}\Big(V_{R_j}\varphi_R(x_j)+V_{L_j}\varphi_L(x_j)\Big)=0, \quad (31a)$$

$$iv_L\Big[\varphi_L(x_j+\epsilon)-\varphi_L(x_j-\epsilon)\Big]+\frac{V_{L_j}}{\omega-\omega_j+i\gamma_j}\Big(V_{L_j}\varphi_L(x_j)+V_{R_j}\varphi_R(x_j)\Big)=0. \quad (31b)$$

Regularizing φ_m by

$$\varphi_m(x)=\lim_{\epsilon\longrightarrow 0}\left[\varphi_m(x_j+\epsilon)+\varphi_m(x_j-\epsilon)\right]/2, \quad (32)$$

and introducing the quantities $\Gamma_{R_j}=V_{R_j}^2/2v_R$ and $\Gamma_{L_j}=V_{L_j}^2/2v_L$, we obtain

$$\varphi_R(x_j+\epsilon)=\left(\frac{\Delta_j-i\Gamma_{R_j}}{\Delta_j+i\Gamma_{R_j}}\right)\varphi_R(x_j-\epsilon)-i\sqrt{\frac{v_L}{v_R}}\frac{\sqrt{\Gamma_{R_j}\Gamma_{L_j}}}{\Delta_j+i\Gamma_{R_j}}\Big(\varphi_L(x_j+\epsilon)+\varphi_L(x_j-\epsilon)\Big), \quad (33a)$$

$$\varphi_L(x_j+\epsilon)=\left(\frac{\Delta_j+i\Gamma_{L_j}}{\Delta_j-i\Gamma_{L_j}}\right)\varphi_L(x_j-\epsilon)+i\sqrt{\frac{v_R}{v_L}}\frac{\sqrt{\Gamma_{L_j}\Gamma_{R_j}}}{\Delta_j-i\Gamma_{L_j}}\Big(\varphi_R(x_j+\epsilon)+\varphi_R(x_j-\epsilon)\Big), \quad (33b)$$

where $\Delta_j=\omega-\omega_j-i\gamma_j$. Using Eq. (29) and (30) we obtain the recursion relations

$$t_j=\left(\frac{\Delta_j-i\Gamma_{R_j}}{\Delta_j+i\Gamma_{R_j}}\right)t_{j-1}-i\sqrt{\frac{v_L}{v_R}}\frac{\sqrt{\Gamma_{R_j}\Gamma_{L_j}}}{\Delta_j+i\Gamma_{R_j}}\Big(r_j e^{-i(q_R+q_L)x_j}+r_{j+1}e^{-i(q_R+q_L)x_j}\Big), \quad (34a)$$

$$r_{j+1}=\left(\frac{\Delta_j+i\Gamma_{L_j}}{\Delta_j-i\Gamma_{L_j}}\right)r_j+i\sqrt{\frac{v_R}{v_L}}\frac{\sqrt{\Gamma_{L_j}\Gamma_{R_j}}}{\Delta_j-i\Gamma_{L_j}}\Big(t_j e^{i(q_R+q_L)x_j}+t_{j-1}e^{i(q_R+q_L)x_j}\Big). \quad (34b)$$

Next, we write transmission and reflection coefficients in terms of the free propagation phase accumulated by the photon as it propagates through the waveguide between two consecutive emitters:

$$t_j=\widetilde{t}_j e^{-i(q_R+q_L)x_j/2}, \quad r_j=\widetilde{r}_j e^{i(q_R+q_L)x_{j-1}/2}, \quad (35)$$

which defines $\widetilde{r}_j$ and $\widetilde{t}_j$. After some rearrangement, (34) can be expressed in the form of the matrix recursion relation

$$\begin{pmatrix}\widetilde{t}_j\\ \widetilde{r}_{j+1}\end{pmatrix}=\mathcal{T}_j\begin{pmatrix}\widetilde{t}_{j-1}\\ \widetilde{r}_j\end{pmatrix}. \quad (36)$$

Here the transfer matrix $\mathcal{T}_j$ is given by

$$\mathcal{T}_j=\begin{pmatrix}e^{i\phi_j}/s_j^* & -p_j^*/s_j^* e^{-i\phi_j}\\ -p_j e^{i\phi_j}/s_j & e^{-i\phi_j}/s_j\end{pmatrix}, \quad (37)$$

where

$$s_j=\frac{\Delta_j-i(\Gamma_{R_j}-\Gamma_{L_j})}{\Delta_j+i(\Gamma_{R_j}+\Gamma_{L_j})}, \quad p_j=\frac{-2i\sqrt{\Gamma_{R_j}\Gamma_{L_j}}}{\Delta_j+i(\Gamma_{R_j}+\Gamma_{L_j})}, \quad \phi_j=(q_R+q_L)(x_j-x_{j-1})/2. \quad (38)$$

Note that using the above transfer matrix formalism, we recover the results of Shen and Fan [38, 46] in the special case $\Gamma_{R_j} = \Gamma_{L_j}$, corresponding to a symmetric waveguide. The net transfer matrix M of the N atom system is given by

$$M = \prod_j \mathcal{T}_j := \begin{pmatrix} M_{11} & M_{12} \\ M_{21} & M_{22} \end{pmatrix}. \tag{39}$$

The net transmission coefficient is given by the formula $T = |t_N|^2$ and the reflection coefficient is then $R = |r_1|^2$. Note that $0 \leq T \leq 1$ since $0 \leq |t_j|^2 \leq 1$ for all j. Alternatively, when $\gamma = 0$, it can be seen that $T = |1/M_{22}|^2$, which is a general property of transfer matrices [43].

IV. BAND STRUCTURE

In this section we consider the band structure that arises for periodic arrangements of atoms in bidirectional waveguides. We begin by focusing on single photon dispersion properties and then consider the effects of back reflections (deviations from chirality). See [18, 20, 38] for the case of symmetric waveguides.

A. Dispersion relation

To study the dispersion characteristics of a single photon, we invoke the periodicity of the infinite lattice and consider solutions of the form

$$\widetilde{t}_j = te^{ijKL} \text{ and } \widetilde{r}_{j+1} = re^{ijKL}, \tag{40}$$

where K is the wavenumber and L is the lattice spacing. By inserting these solutions in (36), we find

$$\begin{pmatrix} t \\ r \end{pmatrix} = e^{-iKL}\mathcal{T}\begin{pmatrix} t \\ r \end{pmatrix}, \tag{41}$$

which means that e^{iKL} is an eigenvalue of $\mathcal{T}$. Thus

$$\det(\mathcal{T} - e^{iKL}\mathcal{I}) = 0, \tag{42}$$

where $\mathcal{I}$ is the 2×2 identity matrix. Eq.(42) becomes, for $\gamma = 0$, the dispersion relation

$$\cos(KL) = \frac{\{\Delta^2 - (\Gamma_R^2 - \Gamma_L^2)\}\cos(q_R + q_L)L/2 + 2\Delta\Gamma_R \sin(q_R + q_L)L/2}{\Delta^2 + (\Gamma_R - \Gamma_L)^2}. \tag{43}$$

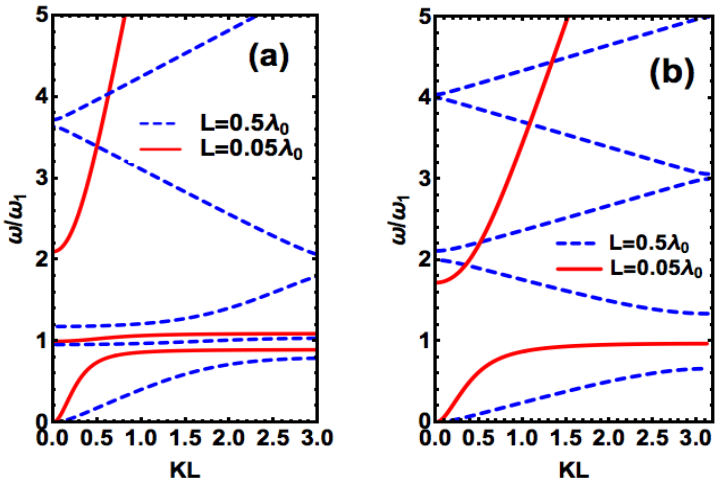

FIG. 5: (Color online) Dispersion relations for two different inter-atomic separations. (a) Small back reflections: the parameters are $\gamma = 0$, $\Gamma_R = 0.1\omega_1$, $v_L = 10v_R$ ($\Gamma_L = 0.1\Gamma_R$) and lattice constant $L = 0.5\lambda$ where $\lambda \equiv 2\pi v_R/\omega_1$. (b) Symmetric waveguides: the parameters are $\gamma = 0, \Gamma = 0.1\omega_1$ and lattice constant $L = 0.5\lambda$.

This result agrees with [19, 20] for the case of symmetric waveguides with $\Gamma_R = \Gamma_L$.

In Fig. 5(a) we consider small back reflections and plot the dispersion relation for two inter-atomic separations. We observe that larger inter-atomic separations create a larger number of branches. In particular, for larger separations a tiny window of forbidden bands opens up. A similar but wider band gap arises for smaller inter-atomic separations. We see that even a small chiral imbalance can produce sufficient destructive interference to form forbidden bands. Moreover, smaller inter-atomic separations produce bigger gaps.

In Fig. 5(b) we plot the dispersion relation for symmetric waveguides. In this situation the dispersion relation (43) becomes

$$\cos(KL) = \cos(qL) + \frac{2\Gamma}{\Delta}\sin(qL), \tag{44}$$

where $q_R = q_L = q$. Similar to the case of small back reflections, we note that the band gap structure can be engineered by altering the separation between the atoms. Beyond this general feature, in the symmetric case, the width and the locations of the band gaps are considerably changed. For instance, the tiny forbidden gap appearing at $\sim 1.2\omega_1$ for small back reflections has been shifted to $\sim 2\omega_1$ for the symmetric problem, where ω_1 is the transition frequency. Moreover, when we compare Fig. 5(a) and Fig. 5(b), we see that the dispersion curve appearing at $\omega = \omega_1$ with $KL \lesssim 0.5$ for the small back reflection problem

does not appear.

B. Small back reflections

We consider a bidirectional waveguide with small back reflections ($\Gamma_R \gg \Gamma_L$). In Fig. 6(a), (b) and (c), we plot the transmission and reflection coefficients T and R as a function of frequency and the number of atoms. For the single-atom case, we find that due to the small atom-waveguide interaction in the backwards (left) direction, T is very large at resonance. However, for the case of multiple atoms a band structure is formed. When $N = 100$, the band gaps are clearly visible and the specific range of frequencies on and near resonance where transmission is completely suppressed can be seen.

C. Symmetric waveguides

We now consider the case of symmetric waveguides with equal group velocities ($\Gamma_L = \Gamma_R$). In this situation, the atom excitation, transmission and reflection amplitudes for the single atom problem simplify to

$$a = \frac{\sqrt{2v\Gamma}}{\Delta + 2i\Gamma}, \quad t = \frac{\Delta}{\Delta + 2i\Gamma}, \quad r = \frac{-2i\Gamma}{\Delta + 2i\Gamma}. \tag{45}$$

In Fig. 7 we plot the transport properties of the system. In the single atom case, the net reflection coefficient manifests a Lorentzian profile with unit value of R at resonance. In the multiple atom scenarios, a full photonic band gap emerges, which allows for the possibility of generating frequency comb patterns [47]. However, as compared to the case of small back reflections, the width of the gap is larger on resonance. For $N = 10$, the off-resonance bands appear as thin peaks with decreasing heights as we move away from resonance.

V. EFFECTS OF DISORDER

A. Evidence for localization

For chiral waveguides, we were able to establish the existence of localization and calculate the localization length analytically. However, for bidirectional waveguides an analysis along the same lines is not straightforward. Instead, we seek numerical evidence for localization

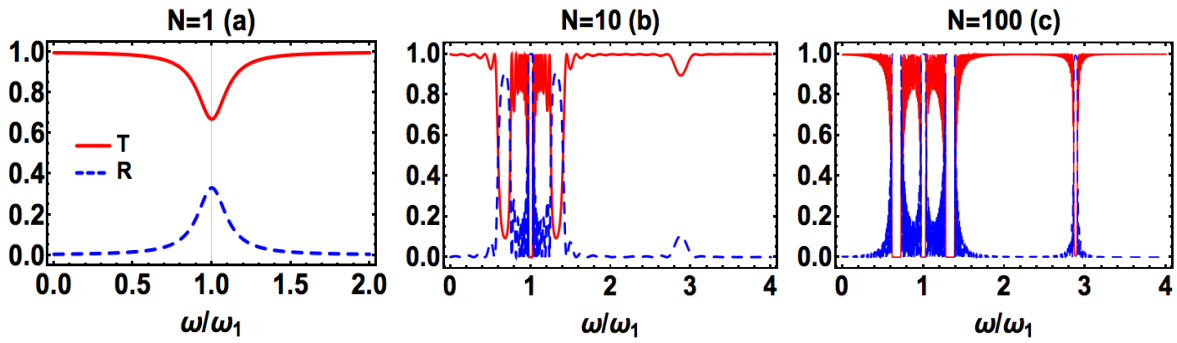

FIG. 6: (Color online) Single-photon transmission and reflection in a waveguide with small back reflections. (a) 1, (b) 10 and (c) 100 periodically arranged identical atoms. The parameters are $\gamma = 0$, $\Gamma_R = 0.1\omega_1$, $v_L = 10v_R$ ($\Gamma_L = 0.1\Gamma_R$) and lattice constant $L = 0.5\lambda$.

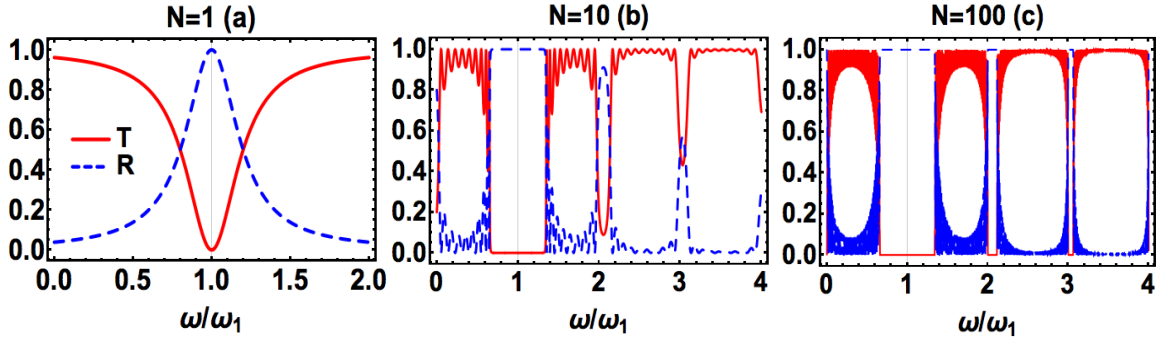

FIG. 7: (Color online) Single-photon transmission and reflection in a symmetric waveguide. (a) 1, (b) 10, and (c) 100 periodically arranged identical atoms. The parameters are $\gamma = 0, \Gamma = 0.1\omega_1$ and lattice constant $L = 0.5\lambda$.

by following (20) and plotting $\langle \ln T \rangle$ as a function of the number atoms N. In Fig. 8 we consider four cases that we will study in detail in later sections: position disorder in symmetric waveguides or with small back reflections, and frequency disorder in symmetric waveguides or with small back reflections. For position disorder (Fig. 8(a) and (b)) we have taken the mean atomic separation to be $\lambda/2$ with disorder strength $\sigma = \lambda$ and fixed atomic transition frequency ω_1. For frequency disorder (Fig. 8(c)), we consider an off resonant situation with mean transition frequency $2\Gamma_R$ for small back reflections and Γ for symmetric waveguides. The disorder strength σ is set to be $\Gamma_R(\Gamma)$. Moreover, a periodic lattice of atoms is considered with $L = \lambda/2$. In all cases, we see that $\langle \ln T \rangle$ decreases linearly with

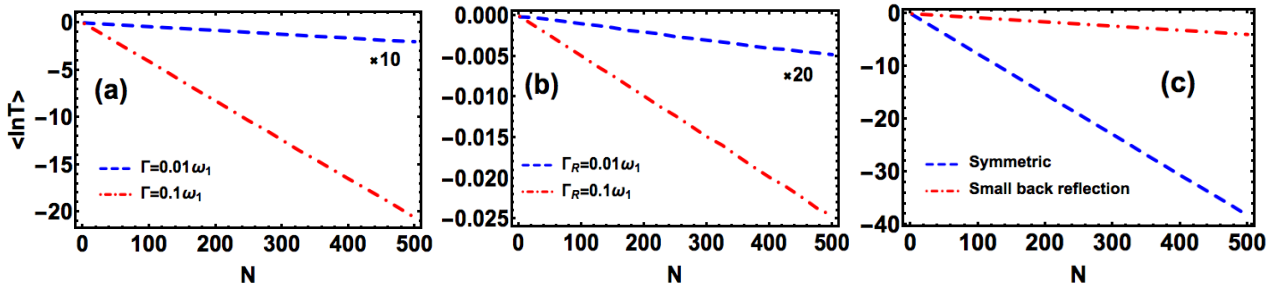

FIG. 8: (Color online) Dependence of $\langle \ln T \rangle$ on the number of atoms N for position disorder. Here $\omega = 2\omega_1$ for (a) symmetric waveguide and (b) small back reflections with $\Gamma_L = 0.1\Gamma_R$ is considered. The mean interatomic separation is $\lambda/2$ and the strength of the disorder $\sigma = \lambda$. (c) Frequency disorder. A periodic chain of atoms is considered with a lattice constant $L = \lambda/2$. The strength of the disorder for small back reflections (symmetric waveguides) is $\sigma = \Gamma_R$ (Γ) and the mean is $2\Gamma_R$ (2Γ). We have set $\gamma = 0$ (no spontaneous decay) and performed the average over 10^4 realizations of the disorder. The error bars are too small to be displayed.

N, consistent with (20). Based on this result, we compute the localization length according to (20).

B. Small back reflections

1. *Position disorder*

We begin by considering a position-disordered 10 atom chain. In Fig. 9(a), we see that the band structure observed in the corresponding periodic setting has disappeared (for comparison see Fig. 6(b)). In addition, on resonance a small region of minimal transmission forms. In Fig. 9(b) we plot the localization length ξ as a function of frequency ω. We find that ξ reaches its minimum value at resonance, where the system is almost completely reflecting. Far from resonance, ξ is considerably enhanced due to the increased transmission. These trends suggest the possibility of forming frequency-dependent localized states due to small back reflections. In Fig. 9(c) we consider a position-disordered chain with $N = 10^3$ atoms. We plot the dependence of the localization length ξ on the strength of disorder σ. We assume that the system is tuned away from resonance (to allow transmission) and

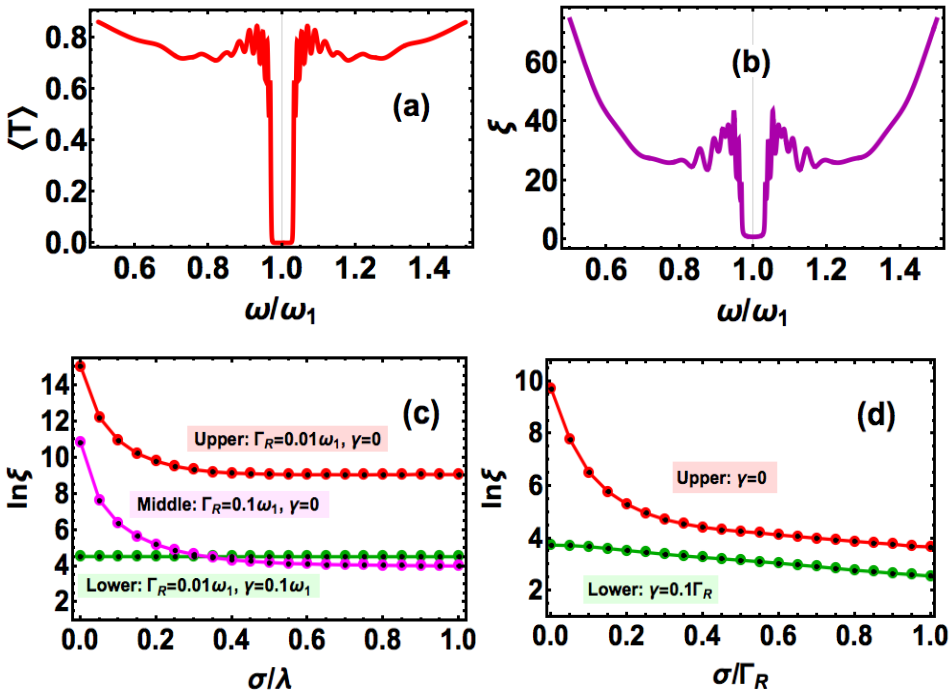

FIG. 9: (Color online) Localization with small back reflections. In all plots $v_L = 10v_R$ (equivalently $\Gamma_L = 0.1\Gamma_R$). In (a) and (b) $\gamma = 0$, $N = 10$, the mean spacing is $\lambda/2$ and the disorder strength $\sigma = 2\lambda$. The average is performed over 500 realizations of the disorder. (a) Average transmission $\langle T\rangle$ as a function of frequency ω for position disorder. (b) Localization length ξ versus ω for position disorder. (c) Localization length ξ versus σ for position disorder. The atomic spontaneous emission rate γ and atom-waveguide coupling rate Γ_R have been varied in different curves. Here the mean spacing is $\lambda/2$, $\omega = 1.6\omega_1$, $N = 10^3$ and 10^4 realizations. (d) ξ versus σ for frequency disorder while varying atomic spontaneous emission rate γ. The atomic spacing is set to be $\lambda/2$, mean frequency is $3\Gamma_R$, $N = 10^3$ and number of realizations is 10^4.

consider the cases of weak and strong coupling of the atoms to the waveguide. We find that ξ is a decreasing function of σ and that ξ is smaller for strong coupling. We also explore the effect of spontaneous emission on ξ. As expected, we find that spontaneous emission is the dominant mechanism to destroy photon transport and the dependence of ξ on σ is very weak.

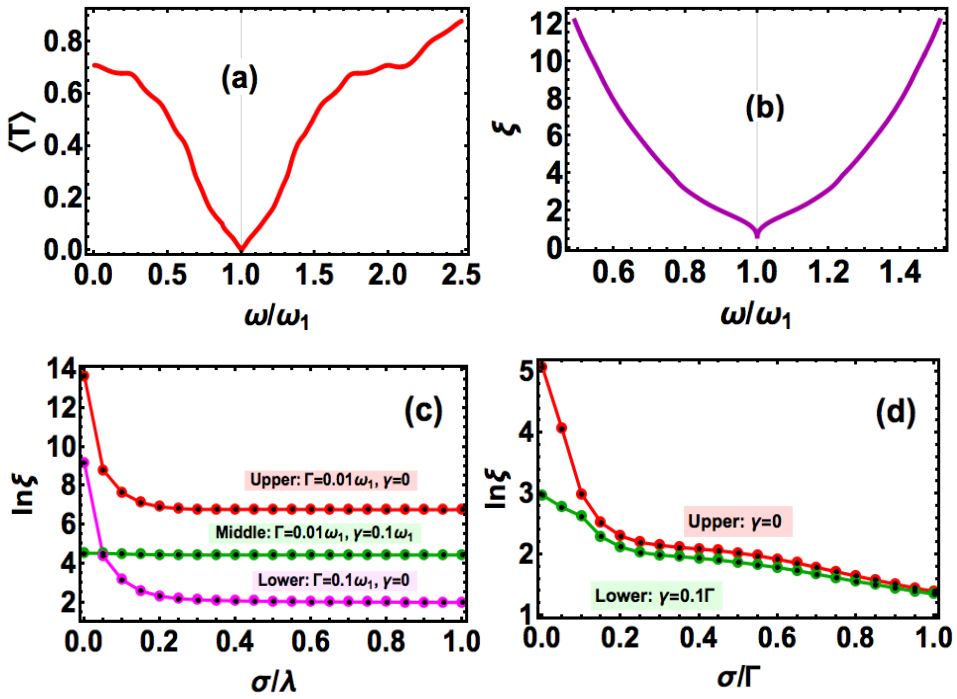

FIG. 10: (Color online) Localization in a symmetric waveguide. The parameters are the same as in Fig. 9.

2. Frequency disorder

In Fig. 9(d) we plot ξ versus σ for frequency disorder. The system is taken far from resonance and shows large transmission for small disorder with $\gamma = 0$. For $\gamma \neq 0$ the transmission remains very small for all values of σ. The overall behavior is similar to that of position disorder.

C. Symmetric waveguides

We now consider the case of symmetric waveguides, following along the same lines as the discussion of waveguides with small back reflections. The results are presented in Fig. 10. We see that the behavior of the transmission and localization length mirrors that in Fig. 9. However, it is important to note that for symmetric waveguides, the scale of ξ is decreased by an order of magnitude compared to waveguides with small back reflections. We also note that if the frequency of the photon ω lies in a bandgap of the corresponding periodic system, then the dependence of the localization length on the strength of the disorder is generally

not decreasing (data not shown).

Our results exhibit similarities and differences compared to studies of photon localization reported in other quantum optical settings. For instance, Schwartz et al. [28] and Lehini et al. [27] have experimentally shown that an increase in the strength of disorder can transform extended states into exponentially localized states in a one-dimensional array of waveguides. Similarly, Javedi et al. [39] have discussed the emission profile of InAs quantum dots in disordered photonic crystal waveguides. They have experimentally demonstrated the enhancement of the Purcell factor by an order of magnitude when the quantum dot is in resonance with an Anderson localized mode. The general feature of suppression of transmission due to increasing disorder strength [27] is also present in our waveguide QED system. However, the question of how chirality [30] influences the formation of localized states is a novel aspect of this problem.

VI. DISCUSSION

We have investigated the problem of single-photon transport in chiral and non-chiral waveguide QED. We have considered the band structure that arises from periodically arranged atoms and have studied the effects of disorder in atomic positions and transition frequencies. Our conclusions may be summarized as follows.

The absence of backscattering in chiral waveguides precludes the existence of band structure in periodic systems. In addition, chiral systems are immune to position disorder and do not exhibit localization. However, localization does arise in chiral waveguides with frequency disorder, a setting in which it is possible to calculate the average transmission and localization length analytically.

Bidirectional waveguides generally exhibit a band structure for periodic systems. The width and location of the bands is controlled by the symmetry of the waveguide. We have found that both positional and frequency disorder lead to localization and that the localization length takes the smallest value at resonance for both types of bidirectional waveguides. For position disorder, strong atom-waveguide coupling generally leads to smaller localization lengths compared to systems with weak coupling. Similar to other quantum optical studies, we have found that the effect of disorder is to decrease transport, which in this work relates to the interplay between disorder and chirality.

ACKNOWLEDGMENTS

This work was supported in part by the NSF grants DMR-1120923 and DMS-1619907.

---

[1] C. Gardiner and P. Zoller in *The Quantum World of Ultra-Cold Atoms and Light Book I: Foundations of Quantum Optics*, pp. 1–328, World Scientific, 2015.

[2] A. Ourjoumtsev, A. Kubanek, M. Koch, C. Sames, P. W. Pinkse, G. Rempe, and K. Murr, "Observation of squeezed light from one atom excited with two photons," *Nature*, vol. 474, no. 7353, pp. 623–626, 2011.

[3] S. Murmann, F. Deuretzbacher, G. Zürn, J. Bjerlin, S. M. Reimann, L. Santos, T. Lompe, and S. Jochim, "Antiferromagnetic heisenberg spin chain of a few cold atoms in a one-dimensional trap," *Physical review letters*, vol. 115, no. 21, p. 215301, 2015.

[4] J. Javanainen, J. Ruostekoski, B. Vestergaard, and M. R. Francis, "One-dimensional modeling of light propagation in dense and degenerate samples," *Physical Review A*, vol. 59, no. 1, p. 649, 1999.

[5] S. Jennewein, M. Besbes, N. Schilder, S. Jenkins, C. Sauvan, J. Ruostekoski, J.-J. Greffet, Y. Sortais, and A. Browaeys, "Coherent scattering of near-resonant light by a dense microscopic cold atomic cloud," *Physical Review Letters*, vol. 116, no. 23, p. 233601, 2016.

[6] B. Zhu, J. Cooper, J. Ye, and A. M. Rey, "Light scattering from dense cold atomic media," *Physical Review A*, vol. 94, no. 023612, 2016.

[7] A. F. Koenderink, A. Alù, and A. Polman, "Nanophotonics: Shrinking light-based technology," *Science*, vol. 348, no. 6234, pp. 516–521, 2015.

[8] R. Blatt and C. Roos, "Quantum simulations with trapped ions," *Nature Physics*, vol. 8, no. 4, pp. 277–284, 2012.

[9] P. Lodahl, S. Mahmoodian, S. Stobbe, A. Rauschenbeutel, P. Schneeweiss, J. Volz, H. Pichler, and P. Zoller, "Chiral quantum optics," *Nature*, vol. 541, no. 7638, pp. 473–480, 2017.

[10] I. M. Mirza and J. C. Schotland, "Multi-qubit entanglement in bi-directional chiral waveguide qed," *Physical Review A*, vol. 94, no. 012302, 2016.

[11] I. M. Mirza and J. C. Schotland, "Two-photon entanglement in multiqubit bidirectional-waveguide qed," *Physical Review A*, vol. 94, no. 1, p. 012309, 2016.

[12] Y.-L. L. Fang, H. U. Baranger, *et al.*, "Waveguide qed: Power spectra and correlations of two photons scattered off multiple distant qubits and a mirror," *Physical Review A*, vol. 91, no. 5, p. 053845, 2015.

[13] A. Goban, C.-L. Hung, J. Hood, S.-P. Yu, J. Muniz, O. Painter, and H. Kimble, "Superradiance for atoms trapped along a photonic crystal waveguide," *Physical review letters*, vol. 115, no. 6, p. 063601, 2015.

[14] A. Asenjo-Garcia, M. Moreno-Cardoner, A. Albrecht, H. Kimble, and D. Chang, "Exponential improvement in photon storage fidelities using subradiance and" selective radiance" in atomic arrays," *arXiv preprint arXiv:1703.03382*, 2017.

[15] J.-t. Shen and S. Fan, "Coherent photon transport from spontaneous emission in one-dimensional waveguides," *Optics letters*, vol. 30, no. 15, pp. 2001–2003, 2005.

[16] D. Witthaut and A. S. Sørensen, "Photon scattering by a three-level emitter in a one-dimensional waveguide," *New Journal of Physics*, vol. 12, no. 4, p. 043052, 2010.

[17] M. Marcuzzi, J. Minář, D. Barredo, S. de Léséleuc, H. Labuhn, T. Lahaye, A. Browaeys, E. Levi, and I. Lesanovsky, "Facilitation dynamics and localization phenomena in rydberg lattice gases with position disorder," *Physical Review Letters*, vol. 118, no. 6, p. 063606, 2017.

[18] M. F. Yanik, W. Suh, Z. Wang, and S. Fan, "Stopping light in a waveguide with an all-optical analog of electromagnetically induced transparency," *Physical review letters*, vol. 93, no. 23, p. 233903, 2004.

[19] J.-T. Shen, M. Povinelli, S. Sandhu, and S. Fan, "Stopping single photons in one-dimensional circuit quantum electrodynamics systems," *Physical Review B*, vol. 75, no. 3, p. 035320, 2007.

[20] D. Zueco, J. J. Mazo, E. Solano, and J. J. García-Ripoll, "Microwave photonics with josephson junction arrays: negative refraction index and entanglement through disorder," *Physical Review B*, vol. 86, no. 2, p. 024503, 2012.

[21] P. W. Anderson, "Absence of diffusion in certain random lattices," *Physical review*, vol. 109, no. 5, p. 1492, 1958.

[22] S. John, "Electromagnetic absorption in a disordered medium near a photon mobility edge," *Physical Review Letters*, vol. 53, no. 22, p. 2169, 1984.

[23] A. Chabanov, M. Stoytchev, and A. Genack, "Statistical signatures of photon localization," *Nature*, vol. 404, no. 6780, pp. 850–853, 2000.

[24] T. Pertsch, U. Peschel, J. Kobelke, K. Schuster, H. Bartelt, S. Nolte, A. Tünnermann, and F. Lederer, "Nonlinearity and disorder in fiber arrays," *Physical review letters*, vol. 93, no. 5, p. 053901, 2004.

[25] P. W. Anderson, "The question of classical localization a theory of white paint?," *Philosophical Magazine B*, vol. 52, no. 3, pp. 505–509, 1985.

[26] L. Sapienza, H. Thyrrestrup, S. Stobbe, P. D. Garcia, S. Smolka, and P. Lodahl, "Cavity quantum electrodynamics with anderson-localized modes," *Science*, vol. 327, no. 5971, pp. 1352–1355, 2010.

[27] M. Segev, Y. Silberberg, and D. N. Christodoulides, "Anderson localization of light," *Nature Photonics*, vol. 7, no. 3, pp. 197–204, 2013.

[28] D. S. Wiersma, "Disordered photonics," *Nature Photonics*, vol. 7, no. 3, pp. 188–196, 2013.

[29] J. D. Joannopoulos, S. G. Johnson, J. N. Winn, and R. D. Meade, *Photonic crystals: molding the flow of light*. Princeton university press, 2011.

[30] R. Coles, D. Price, J. Dixon, B. Royall, E. Clarke, P. Kok, M. Skolnick, A. Fox, and M. Makhonin, "Chirality of nanophotonic waveguide with embedded quantum emitter for unidirectional spin transfer," *Nature communications*, vol. 7, 2016.

[31] J. Petersen, J. Volz, and A. Rauschenbeutel, "Chiral nanophotonic waveguide interface based on spin-orbit interaction of light," *Science*, vol. 346, no. 6205, pp. 67–71, 2014.

[32] I. Söllner, S. Mahmoodian, S. L. Hansen, L. Midolo, A. Javadi, G. Kiršanskė, T. Pregnolato, H. El-Ella, E. H. Lee, J. D. Song, *et al.*, "Deterministic photon–emitter coupling in chiral photonic circuits," *Nature nanotechnology*, vol. 10, no. 9, pp. 775–778, 2015.

[33] R. Mitsch, C. Sayrin, B. Albrecht, P. Schneeweiss, and A. Rauschenbeutel, "Quantum state-controlled directional spontaneous emission of photons into a nanophotonic waveguide," *Nature communications*, vol. 5, 2014.

[34] E. E. Hach III, A. W. Elshaari, and S. F. Preble, "Fully quantum-mechanical dynamic analysis of single-photon transport in a single-mode waveguide coupled to a traveling-wave resonator," *Physical Review A*, vol. 82, no. 6, p. 063839, 2010.

[35] A. Akimov, A. Mukherjee, C. Yu, D. Chang, A. Zibrov, P. Hemmer, H. Park, and M. Lukin, "Generation of single optical plasmons in metallic nanowires coupled to quantum dots," *Nature*, vol. 450, no. 7168, pp. 402–406, 2007.

[36] O. Astafiev, A. M. Zagoskin, A. Abdumalikov, Y. A. Pashkin, T. Yamamoto, K. Inomata, Y. Nakamura, and J. Tsai, "Resonance fluorescence of a single artificial atom," *Science*, vol. 327, no. 5967, pp. 840–843, 2010.

[37] A. Sipahigil, R. Evans, D. Sukachev, M. Burek, J. Borregaard, M. Bhaskar, C. Nguyen, J. Pacheco, H. Atikian, C. Meuwly, *et al.*, "An integrated diamond nanophotonics platform for quantum-optical networks," *Science*, vol. 354, no. 6314, pp. 847–850, 2016.

[38] J.-T. Shen and S. Fan, "Coherent single photon transport in a one-dimensional waveguide coupled with superconducting quantum bits," *Physical review letters*, vol. 95, no. 21, p. 213001, 2005.

[39] A. Javadi, S. Maibom, L. Sapienza, H. Thyrrestrup, P. D. García, and P. Lodahl, "Statistical measurements of quantum emitters coupled to anderson-localized modes in disordered photonic-crystal waveguides," *Optics express*, vol. 22, no. 25, pp. 30992–31001, 2014.

[40] A. Crespi, R. Osellame, R. Ramponi, V. Giovannetti, R. Fazio, L. Sansoni, F. De Nicola, F. Sciarrino, and P. Mataloni, "Anderson localization of entangled photons in an integrated quantum walk," *Nature Photonics*, vol. 7, no. 4, pp. 322–328, 2013.

[41] S. Zhang, F. Robicheaux, and M. Saffman, "Magic-wavelength optical traps for rydberg atoms," *Physical Review A*, vol. 84, no. 4, p. 043408, 2011.

[42] K. Maller, M. Lichtman, T. Xia, Y. Sun, M. Piotrowicz, A. Carr, L. Isenhower, and M. Saffman, "Rydberg-blockade controlled-not gate and entanglement in a two-dimensional array of neutral-atom qubits," *Physical Review A*, vol. 92, no. 2, p. 022336, 2015.

[43] P. Markos and C. M. Soukoulis, *Wave propagation: from electrons to photonic crystals and left-handed materials*. Princeton University Press, 2008.

[44] F. Izrailev and A. Krokhin, "Localization and the mobility edge in one-dimensional potentials with correlated disorder," *Physical review letters*, vol. 82, no. 20, p. 4062, 1999.

[45] D. Delande, K. Sacha, M. Płodzień, S. K. Avazbaev, and J. Zakrzewski, "Many-body anderson localization in one-dimensional systems," *New Journal of Physics*, vol. 15, no. 4, p. 045021, 2013.

[46] S. Fan, "Sharp asymmetric line shapes in side-coupled waveguide-cavity systems," *Applied Physics Letters*, vol. 80, no. 6, pp. 908–910, 2002.

[47] Z. Liao, H. Nha, and M. S. Zubairy, "Single-photon frequency-comb generation in a one-dimensional waveguide coupled to two atomic arrays," *Physical Review A*, vol. 93, no. 3,

p. 033851, 2016.